Video Article

Evaluating Plasmonic Transport in Current-carrying Silver Nanowires

Mingxia Song[1], Arnaud Stolz[1], Douguo Zhang[2], Juan Arocas[1], Laurent Markey[1], Gérard Colas des Francs[1], Erik Dujardin[3], Alexandre Bouhelier[1]

[1]Laboratoire Interdisciplinaire Carnot de Bourgogne CNRS-UMR 6303, Université de Bourgogne

[2]Department of Optics and Optical Engineering, University of Science and Technology of China

[3]CEMES, CNRS-UPR 8011

Correspondence to: Alexandre Bouhelier at alexandre.bouhelier@u-bourgogne.fr

URL: https://www.jove.com/video/51048
DOI: doi:10.3791/51048

Keywords: Physics, Issue 82, light transmission, optical waveguides, photonics, plasma oscillations, plasma waves, electron motion in conductors, nanofabrication, Information Transport, plasmonics, Silver Nanowires, Leakage radiation microscopy, Electromigration

Date Published: 12/11/2013

Citation: Song, M., Stolz, A., Zhang, D., Arocas, J., Markey, L., Colas des Francs, G., Dujardin, E., Bouhelier, A. Evaluating Plasmonic Transport in Current-carrying Silver Nanowires. *J. Vis. Exp.* (82), e51048, doi:10.3791/51048 (2013).

Abstract

Plasmonics is an emerging technology capable of simultaneously transporting a plasmonic signal and an electronic signal on the same information support[1,2,3]. In this context, metal nanowires are especially desirable for realizing dense routing networks[4]. A prerequisite to operate such shared nanowire-based platform relies on our ability to electrically contact individual metal nanowires and efficiently excite surface plasmon polaritons[5] in this information support. In this article, we describe a protocol to bring electrical terminals to chemically-synthesized silver nanowires[6] randomly distributed on a glass substrate[7]. The positions of the nanowire ends with respect to predefined landmarks are precisely located using standard optical transmission microscopy before encapsulation in an electron-sensitive resist. Trenches representing the electrode layout are subsequently designed by electron-beam lithography. Metal electrodes are then fabricated by thermally evaporating a Cr/Au layer followed by a chemical lift-off. The contacted silver nanowires are finally transferred to a leakage radiation microscope for surface plasmon excitation and characterization[8,9]. Surface plasmons are launched in the nanowires by focusing a near infrared laser beam on a diffraction-limited spot overlapping one nanowire extremity[5,9]. For sufficiently large nanowires, the surface plasmon mode leaks into the glass substrate[9,10]. This leakage radiation is readily detected, imaged, and analyzed in the different conjugate planes in leakage radiation microscopy[9,11]. The electrical terminals do not affect the plasmon propagation. However, a current-induced morphological deterioration of the nanowire drastically degrades the flow of surface plasmons. The combination of surface plasmon leakage radiation microscopy with a simultaneous analysis of the nanowire electrical transport characteristics reveals the intrinsic limitations of such plasmonic circuitry.

Video Link

The video component of this article can be found at https://www.jove.com/video/51048/

Introduction

Plasmonics aims at merging electronics and photonics in a shared physical support via the mediation of an electron density wave called a surface plasmon polariton[1,2,3]. Surface plasmon can travel in various waveguide geometries and interfaces. Among them, metal nanowires are especially desirable. As quasi-one dimensional structures they drastically confine the plasmon field to deep subwavelength scale while acting as electrical interconnects capable of sustaining an electron flow as depicted by the artistic drawing of **Figure 1**.

Both surface plasmon propagation and electron transport are sensitive to structural inhomogeneities of the nanowire (*e.g.* kinks, crystalline defects, *etc.*). Because they can grow as a single crystal with few defects, chemically-synthesized metal nanowires[6] typically provide improved transport performances over amorphous metal nanowires fabricated by top-down approaches (*e.g.* electron beam lithography)[12]. The realization of a plasmonic network unit cell requires transferring the nanowires from a colloidal solution to a glass substrate. Without any specific complex prepatterning like surface functionalization[13] or self-assembly techniques[14], nanowires are generally randomly oriented on the substrate. This uncontrolled distribution of orientations drastically complicates the electrical connection of the nanowire to an outside power source.

In this article, randomly oriented chemically-synthesized silver nanowires are successfully contacted by source and drain electrical terminals. To this purpose optical microscopy is combined with electron-beam lithography to precisely locate the nanowire and create electrical contacts[15,16]. A characterization procedure evaluating the electro-plasmonic performances of the circuitry is described. After electrode fabrication, the contacted nanowires are transferred to a surface plasmon leakage radiation microscope for analyzing the effect of an electron flow on the propagation of surface plasmons. The microscope uses an inverted base equipped with a high numerical aperture oil-immersion objective and two charge-coupled device (CCD) cameras placed at the conjugate object plane and conjugate Fourier plane, respectively. These two conjugate planes provide complementary information on surface plasmon properties. Details of the propagation are directly inferred from image plane analysis, while the momentum distribution is visualized by Fourier plane imaging[9].

Surface plasmons are excited in an individual nanowire by focusing a near-infrared laser beam in a diffraction-limited spot at the glass/air interface. When a nanowire extremity is aligned inside the focal region, the scattered incident laser light creates a broad distribution of wave-vectors, some of them resonant with the excitation of a surface plasmon. The propagation of this surface wave is visualized either by collecting

the leakage of the mode emitted in the substrate or by observing the plasmon scattered at the nanowire distal end. The propagation length and effective index of the leaky surface plasmon mode are measured by analyzing the intensity distributions in a dual-plane leakage radiation microscopy.

Once a surface plasmon develops in the nanowire, the drain and source terminals at each extremity of the nanowire are connected to a regulated voltage supply. The CCD cameras monitor in real time the surface plasmon properties as a function of current flowing through the nanowire. For each value of the electrical transfer characteristic, the effective index and the propagation length of the surface plasmon mode are determined. This procedure enables to estimate the limitation of a nanowire-based circuitry to simultaneously sustain the transport of electrons and plasmons[7].

Protocol

1. Synthesis of a Colloidal Solution of Silver Nanowires

Silver nanowires (Ag NWs) with smooth surface and homogeneous structure are synthesized using a modified polyols-assisted method[6]. In a typical synthesis of Ag NWs, the following procedures are carried out step by step:

1. Pour 12 ml ethylene glycol (EG) in a 100 ml precleaned, round-bottomed capped flask.
2. Heat the solution at 150 °C for 1 hr in the oil bath (dimethylsilicone) with magnetic stirring at 260 rpm.
3. Add 4 ml $AgNO_3$ (0.2 M in EG solution) by dropping. During this process, the color of the reaction solution changes from colorless to transparent bright yellow, which indicates the growth of silver crystal seeds.
4. Slowly inject 4 ml poly-(vinylpyrrolidone) (PVP) solution (the concentration is 22.2 mg/ml in EG solution) in the reaction solution with a pipette. In the reaction, EG serves as both the solvent and reducing agent, and the PVP enables the silver single crystal to grow along a certain direction.
5. Cover the reaction flask with a cap. After 150 min, the color of the solution changes from light yellow to sage green. Finally the colloid appears turbid silver-grey.
6. Stop the reaction by placing the flask in an ice-cold water bath to decrease the temperature of the solution.
7. Transfer 1 ml of the colloidal solution to a centrifuge tube filled with 3 ml of acetone.
8. Centrifuge the tube at 600 x g for 25 min.
9. Remove the supernatant and add 4 ml of DI water.
10. Repeat steps 1.8-1.9 at least 3x to remove the excess of EG and PVP.

2. Preparing Macroscopic Alignment Landmarks on a Glass Substrate by Electron-beam Lithography

1. Clean a microscope cover glass N°1 ½ calibrated for oil immersion microscopy in a diluted concentrated soap solution [1:3] using an ultrasonic bath.
2. Rinse first in a large volume of DI water, followed by a second wash with isopropanol. Blow-dry the cover slip with nitrogen.
3. Pipette 160 ml of poly(methyl methacrylate) (PMMA) electron beam resist (see table of reagents) and spin coat it the NW covered substrate with the following successive coating parameters:
    1. 10 sec at a speed of 4 x g and an acceleration of 4 x g/sec.
    2. 1 sec at a speed of 350 x g and an acceleration of 200 x g/sec.
    3. 60 sec at a speed of 700 x g and an acceleration of 200 x g/sec.
4. Bake the sample at 170 °C for 10 min on a hot plate.
5. Repeat steps 2.2-2.4 to produce a second layer of resist to facilitate liftoff at the end of the procedure. Use the same electron-beam resist for both layers.
6. Sputter a thin conductive gold layer (20 nm) on the top of the sample before proceeding to electron beam lithography.
7. Transfer the sample to an electron-beam microscope equipped for lithography. Using a Faraday cage, set the beam current to 150 pA.
8. Expose the sample following the design layout of the grid landmarks with a step size set at 48 nm, a dwell-time per pixel at 0.0243 msec for a dose of 150 $\mu A/cm^2$.
9. Develop the sample using MIBK (methyl isobutyl ketone): IPA (isopropanol) with a ratio [1:3] for 45 sec. Stop the process by dipping the sample in isopropanol for another 45 sec.
10. Transfer the substrate in a metal evaporator operating at a base pressure of 8×10^{-8} mbar. Deposit at an evaporation rate of 0.1 nm/sec 2 nm of Cr (adhesion layer) followed by 70 nm of Au.
11. Proceed to a chemical lift-off of the sample using acetone warmed at 70 °C for about 1.5 hr.

3. Deposition of the Nanowires on the Substrate

1. Dilute the nanowire solution in ethanol to obtain a nanowire density on the substrate of about one nanowire every 10 μm^2.
2. Pipette 50 µl of the solution and drop-cast it on the prepatterned substrate. Blow dry with nitrogen.

4. Locating the Nanowires by Optical Microscope

1. Place the substrate decorated with nanowires on a standard calibrated optical microscope.

2. Precisely locate the extremities of a series of isolated high-quality nanowires with respect to the closest alignment marks.

5. Fabrication of the Electrodes by Electron Beam Lithography, Thermal Evaporation, and Chemical Lift-off

1. Use the measured positions of the nanowires to design an electrode layout. Incorporate large receiving pads (50 µm x 50 µm) to connect tungsten voltage probes to the electrode reaching the nanowires.
2. Pipette 160 ml of poly(methyl methacrylate) (PMMA) electron beam resist (see table of reagents) and spin coat the nanowire-covered substrate with the following successive coating parameters:
    1. 10 sec at a speed of 4 x g and an acceleration of 4 x g/sec.
    2. 1 sec at a speed of 350 x g and an acceleration of 200 x g/sec.
    3. 60 sec at a speed of 700 x g and an acceleration of 200 x g/sec.
3. Bake the sample at 170 °C for 10 min on a hot plate.
4. Repeat steps 5.2-5.3 to produce a second layer of resist to facilitate liftoff at the end of the procedure. Use the same electron-beam resist for both layers.
5. Sputter a thin conductive gold layer (20 nm) on the top of the sample before proceeding to electron beam lithography.
6. Transfer the sample to an electron-beam microscope equipped for lithography. Using a Faraday cage, set the beam current to 150 pA.
7. Using the alignment marks, calibrate the coordinate system of the electron-beam microscope.
8. Expose the sample following the design layout with a step size set at 48 nm, a dwell-time per pixel at 0.0243 msec for a dose of 150 µA/cm^2.
9. Develop the sample using MIBK (methyl isobutyl ketone): IPA (isopropanol) with a ratio [1:3] for 45 sec. Stop the process by dipping the developed sample in isopropanol for another 45 sec.
10. Transfer the substrate in a metal evaporator operating at a base pressure of 8 x 10^{-8} mbar. Deposit at an evaporation rate of 0.1 nm/sec, 2 nm of Cr (adhesion layer) followed by 70 nm of Au.
11. Proceed to a chemical lift-off of the sample using acetone warmed at 70 °C for about 1.5 hr.

6. Transfer to a Surface Plasmon Leakage Radiation Microscope

1. Set up a surface plasmon leakage microscope equipped with a high numerical aperture objective (N.A.>1) and a two-axis piezoelectric stage to adjust sample position.
2. Prepare a collimated Gaussian beam from a near-infrared laser. Longer excitation wavelength provides longer plasmon propagation distance. Align the beam in the microscope. The diameter of the collimated beam should overfill the entrance pupil of the microscope. This insures the formation of a diffraction-limited focal spot at the glass/air interface.
3. With the help of beam splitters and a series of relay lenses positioned at one exit port of the microscope, form two planes conjugate with the object plane and with the Fourier plane (objective back focal plane), respectively. Place two charge-coupled device (CCD) cameras at the location of these conjugate planes.
4. Using the piezoelectric stage, align the extremity of a selected contacted nanowire to overlap the focal spot. Adjust the position to maximize light coupling into the plasmon mode.
5. Connect a regulated power supply to the receiving pads of the electrical terminals with tungsten tips mounted on three-dimensional mechanical probers. Insert a low gain current-to-voltage converter (gain 10mA/V) or a current meter in the circuitry.
6. Monitor the applied bias, the current flowing through the nanowire and the intensity distributions recorded by the two CCDs cameras.

Representative Results

Figure 2(a) shows a scanning electron micrograph of a typical 10 mm long Ag nanowire synthesized using the protocol outlined above. The width of the nanowire is here 200 nm as shown in the close up view of the left extremity in **Figure 2(b)**. The figure readily shows the five-fold symmetry of the crystal growth. There are no visible defects on the surface of the nanowire (*e.g.* kinks, particles, *etc.*). The synthesis leads to a large distribution of nanowire lengths and widths. Shorter and smaller nanowires are notably visible around the thickest one in **Figure 2(a)**.

Figure 3 displays typical scanning electron micrographs of the alignment marks lithographed on the glass substrate. The four large alignment marks located at the corners of the writing field (solid arrow) are used to report the coordinate systems between the successive lithography steps. To improve position accuracy in the repositioning, a second alignment is performed with the help of the smaller marks located at the each corner of the grid array (dashed arrow). The labeled crosses at the center of the writing field serve to precisely locate the randomly deposited nanowires with the help of an optical microscope.

Figure 4 shows optical images of silver nanowires deposited on a glass substrate before and after electrode fabrication. A diluted solution of nanowires is transferred to the substrate to avoid a high concentration on the surface that may jeopardize the electrical integrity of the connections. In **Figure 4(a)**, the nanowire location is located with the four alignment marks prepatterned on the substrate (see details of the procedure 2). **Figure 4(b)** shows an image of the same nanowire after electron-beam lithography of the electrodes, subsequent deposition of a 70 nm thick Au layer and a chemical lift-off of the resist. **Figures 4(c)** and **4(d)** show another nanowire before and after fabricating the electrical terminals. The use of gold for forming the contacts over silver brings long-term stability of the fabricated structures; the quality of evaporated Ag layer degrades within a few days. Note that the silver nanowires used in this work have a longer lifetime; the surfactant covering the nanowires slows down the surface degradation by atmospheric contaminants. Other metals with high conductivity like Pd, Pt, or Ti can easily substitute the Au contacts.

A schematic of the leakage radiation microscope used in this work is depicted in **Figure 5**. An inverted microscope is equipped with a high numerical aperture (N.A.) oil immersion objective (N.A.=1.49). The objective produces on one hand the necessary field distribution to excite a surface plasmon developing in the nanowire and collects on the other hand the plasmon leakage and related optical information. A laser source

emitting at 780 nm excites the surface plasmons. Metallic losses in this near-infrared wavelength are significantly reduced compared to visible wavelengths providing thus longer plasmon propagation length. The lateral position of the nanowire and the focal spot are adjusted with the help of three-dimensional piezoelectric-controlled sample stage. Alternatively, galvanometric mirrors can also be utilized to steer the excitation beam. Two CCD cameras record the critical plasmon properties. These cameras are placed in the two conjugate planes of the microscope. A first CCD is placed at a secondary conjugate object plane (II") and records the intensity distribution of the leaky propagating surface plasmon mode. A 4f imaging system with two 100 mm focal length lenses forms a conjugate plane II" of the object. A second 4f imaging system forms a magnified image of the conjugate Fourier plane Σ" of the microscope. The two lenses in this system have focal lengths of L1=100 mm and L2=150 mm. The CCD placed at the Fourier plane Σ" monitors the wave-vector distribution. With this dual-plane leakage radiation imaging, the surface plasmon characteristics such as its effective index and attenuation length are determined. Depending on the nanowire diameter, different surface plasmon modes are excited. The Fourier content of the leaky mode radiating in the substrate features a single line located at the mode effective index. The width of the line is inversely proportional to the propagation length of the surface plasmon[17]. If a bound surface plasmon mode is excited, the numerical aperture of the objective is no longer sufficient to collect the associated in-plane wave-vector. However, the excitation of a bound mode is easily confirmed by an out-coupling of the surface plasmon intensity at the distal nanowire extremity.

Figure 6(a) illustrates the propagation of surface plasmons excited in a bare Ag nanowire without electrical connections. The image is recorded in the object plane II". The focused excitation appears as an intensity-saturated region overlapping with one extremity of the nanowire. The two luminous lines located at either side of the nanowire confirm the radiation leakage of the plasmon during its propagation. **Figure 6(b)** displays the corresponding momentum distribution (k_x/k_o,k_y/k_o) recorded in the Fourier plane Σ". The numerical aperture of the objective (here 1.49) limits the detection window. The inner ring corresponds to the critical angle at the glass/air interface. The line at a constant k_x/k_o in the red box is the signature of the surface plasmon leaky mode. The effective index of the mode N_{eff} is evaluated by fitting the experimental wave-vector profile with a Lorentzian curve. The peak of the curve corresponds to N_{eff} and is here determined at 1.02. The full-width at half-maximum of the Lorentzian curve is inversely proportional to the surface plasmon propagation length[17]. Using this dual plane imaging, the principal properties of the plasmon mode are completely determined.

Figure 7 shows a typical image illustrating the propagation of a leaky surface plasmon mode in an electrically connected Ag nanowire. The white lines indicate the position of the electrodes. The image generally resembles that of **Figure 6(a)** obtained for a plasmon propagating in a nanowire without any electrodes. This strongly suggests that the propagation of the mode is not affected by the presence of the additional metal layer at the electrodes. Note that the mode no longer in the region where the electrodes are in contact with the surface because of the different geometry. However, the plasmon propagation and its associated leakage radiation resume in the bare nanowire after the electrode. **Figure 7(b)** displays the wave-vector distribution of the detected signal; a bright line similar to that observed in **Figure 6(b)** is the signature of the leaky mode. Using the information contained in this dual-plane imaging scheme, the properties of the surface plasmons are then evaluated when a current flow is established in the nanowire.

Figure 8 shows representative results of the evolution of the surface plasmon properties with voltage bias applied at the electrodes. An electronic control of a scanning tunneling microscope delivers the bias voltage and acquires the data. The advantage of using this type of acquisition device is the possibility to generate handshaking synchronization signals with the CCD cameras at each value of the voltage to simultaneously evaluate the transport of electrical current and propagation of surface plasmons. **Figure 8(a)** displays the current-voltage characteristic of the nanowire. For small biases, a linear relationship indicates an ohmic transport. Above approximately 0.4 V, the trend is no longer linear; a temperature-dependent resistance, amorphization of the nanowire and electromigration-induced mass transport affect the electron flow[18]. Electrical failure of the nanowire occurs at 1.2 V. The plasmon effective index N_{eff} and the full-width at Half-Maximum (FWHM) deduced from Fourier plane analysis (see **Figure 6**) are reported for each bias voltage in **Figure 8(b)**. These two plasmon characteristics are independent of voltage as long as the current scales linearly with the bias (<0.4 V). At the onset of electromigration (≈ 1.1 V) N_{eff} decreases significantly. The evolution of N_{eff} results from a modification of the nanowire diameter by the electromigration process[7]. The effective index is varying around 1.027 with voltage and the loss encoded in the FWHM of the Fourier signature follows the evolution of N_{eff}. The variation of these two parameters results from the dynamic morphological change of the nanowire with voltage. Close to the electrical rupture, the plasmon no longer reaches the distal end of the nanowire as shown by **Figure 8(c)**. This is confirmed by the leakage radiation images displayed in **Figures 8(d), 8(e)** and **8(f)**. These images are acquired at different operating conditions reported in **Figure 8(a)** and correspond to a bias-free nanowire (*i*), a current value above the electromigration threshold (*ii*) and after electrical failure (*iii*). The current flow affects both surface plasmon leakage and light scattered at the extremity of the nanowire. After the nanowire structural breakdown at 1.2 V (**Figure 8(f)**), there is no evidence of a surface plasmon launched in this electrically and structurally damaged nanowire.

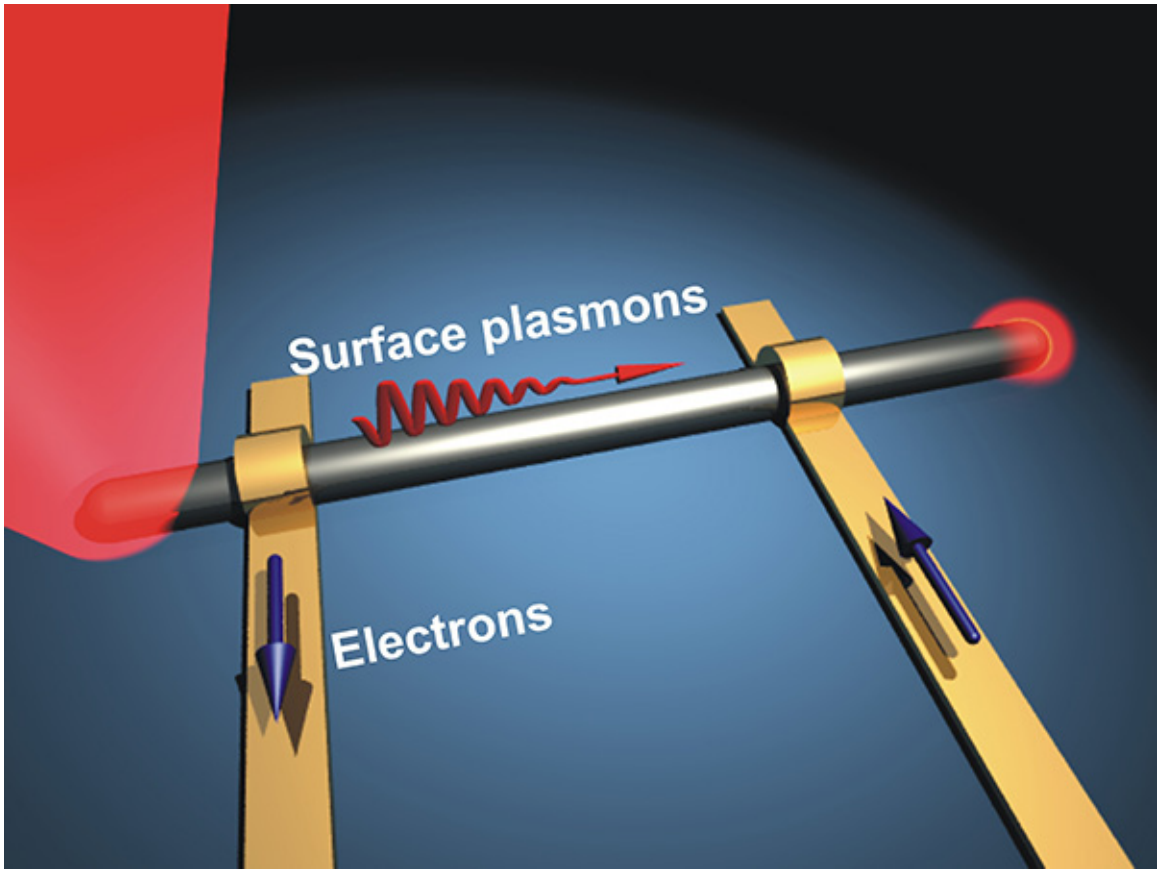

Figure 1. Artistic rendering of a basic plasmonic circuitry. An electrically contacted Ag nanowire simultaneously transports electrons as well as optical information encoded in the form of surface plasmon polaritons. Click here to view larger image.

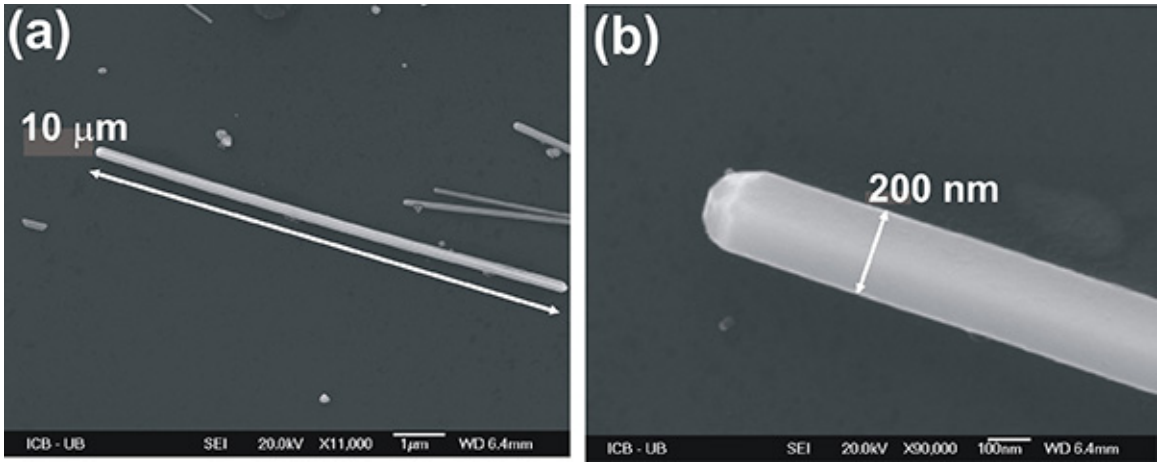

Figure 2. (**a**) **Scanning electron micrograph of a chemically-synthesized silver nanowire drop casted and dried on a substrate.** The nanowire is 10 mm long with a section of 200 nm. (**b**) Close up view of the left termination of the nanowire emphasizing its pentagonal shape. Click here to view larger image.

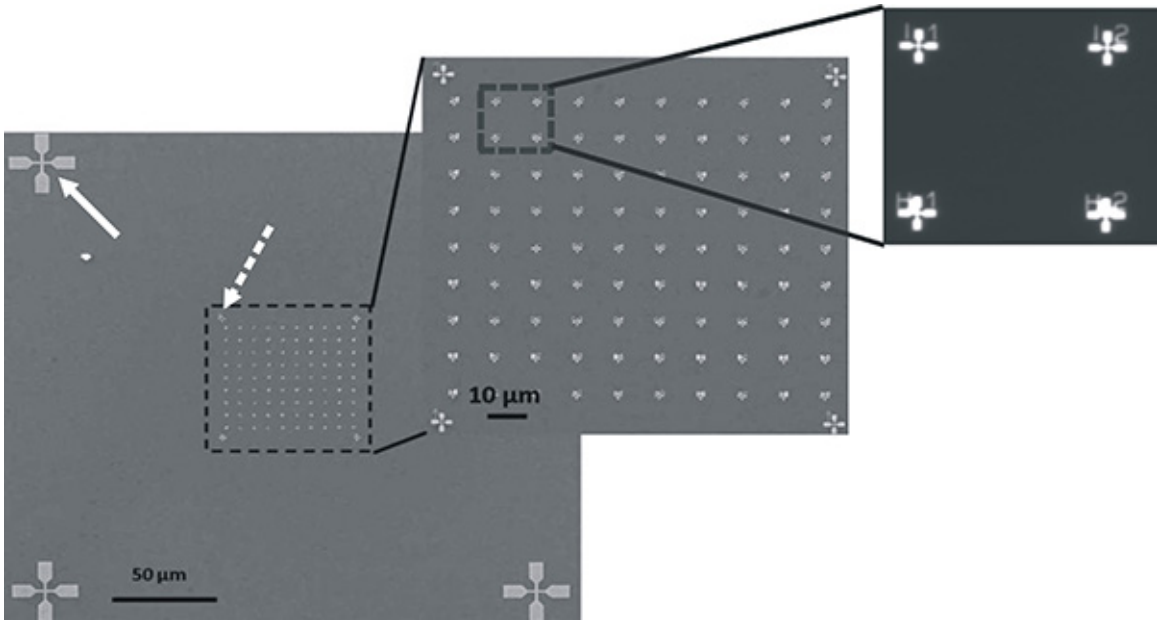

Figure 3. Scanning electron micrographs of the grid landmark pattern at different magnifications. Click here to view larger image.

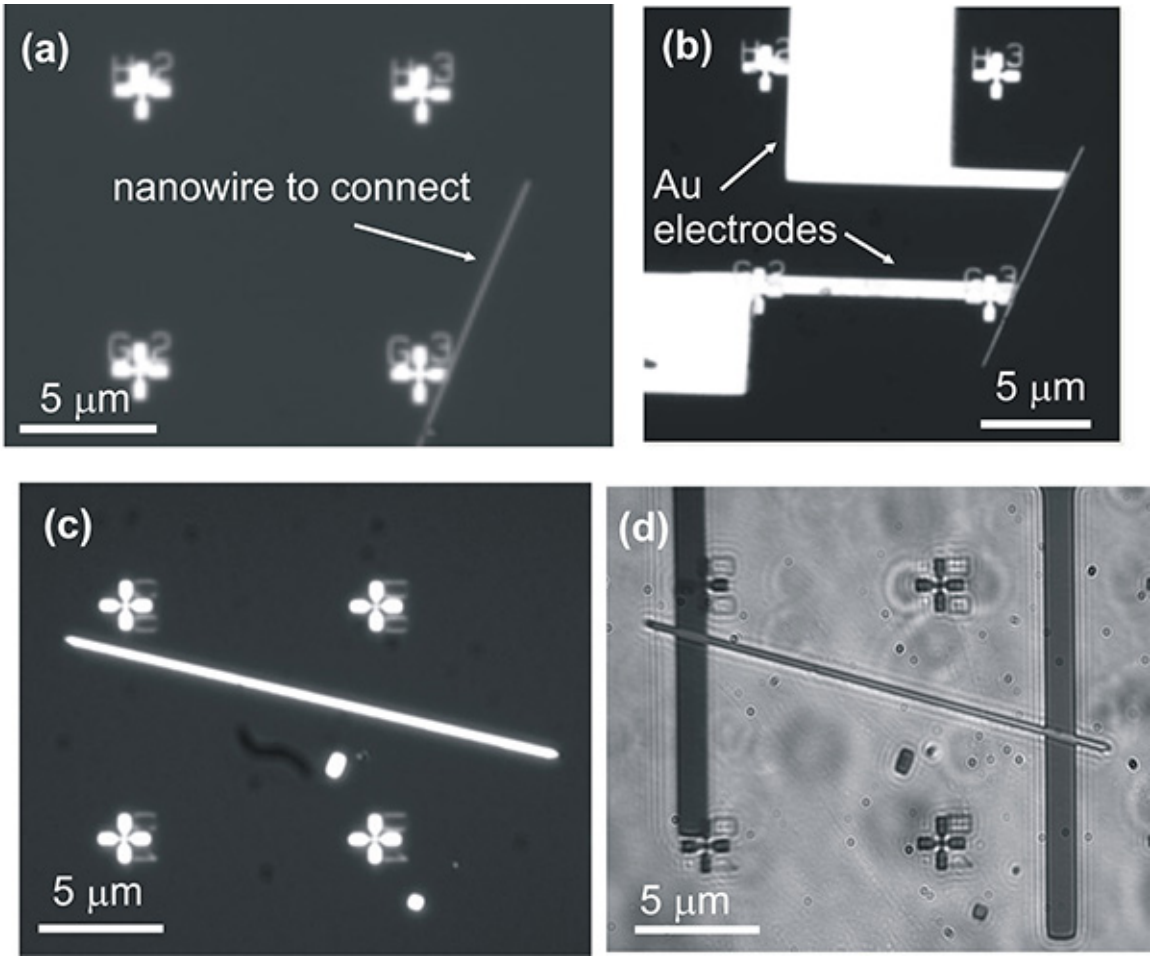

Figure 4. Example of contacted Ag nanowires. (**a**) and (**c**) Isolated silver nanowires randomly deposited in the grid landmarks. (**b**) and (**d**) The same nanowires electrically connected to a set of Au electrodes. The distance between each mark is 10 mm. The electrodes are designed by electron-beam lithography and subsequent chromium (2 nm) and gold (70 nm) depositions. Click here to view larger image.

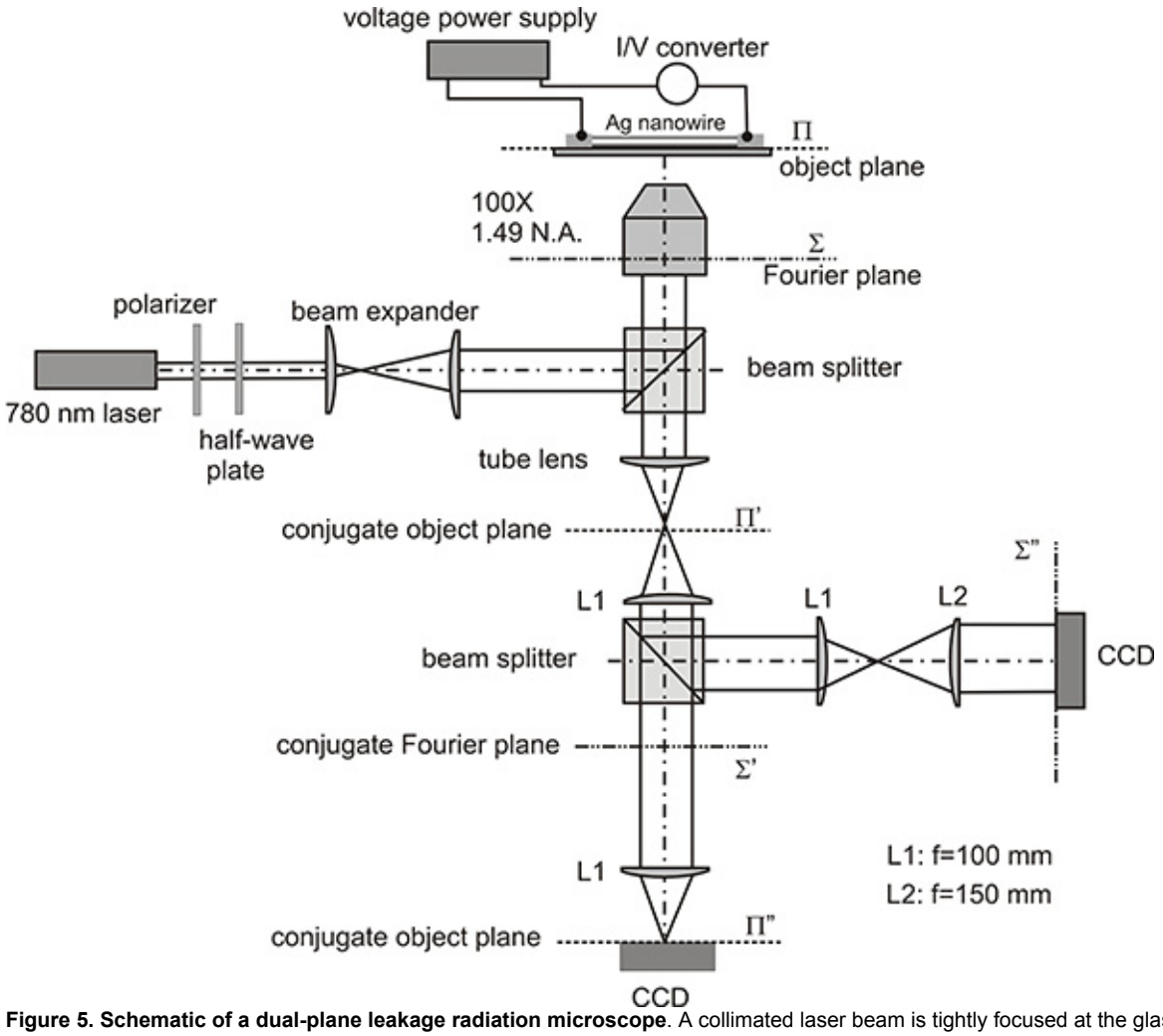

Figure 5. Schematic of a dual-plane leakage radiation microscope. A collimated laser beam is tightly focused at the glass/air interface by a high numerical aperture objective (N.A.=1.49). If a silver nanowire is laterally displaced to have one extremity overlapping the focal spot, a surface plasmon is excited. Depending on the nature of the excited mode, surface plasmon propagation may be seen as leakage radiation along the nanowire or as a light intensity scattered from the distal end. In both cases, the same objective collects the light and sends it to two different conjugate planes S" and P" for CCD recording. The CCD placed at the conjugate image plane P" provides a magnified image of the sample used to visualize the propagation of the surface plasmon. The CCD placed at the conjugate Fourier plane S" measures the wave-vector distribution contained in the plasmon leakage. A regulated power supply provides the bias applied to the nanowire and a home-made current-to-voltage converter monitors the current flowing. Click here to view larger image.

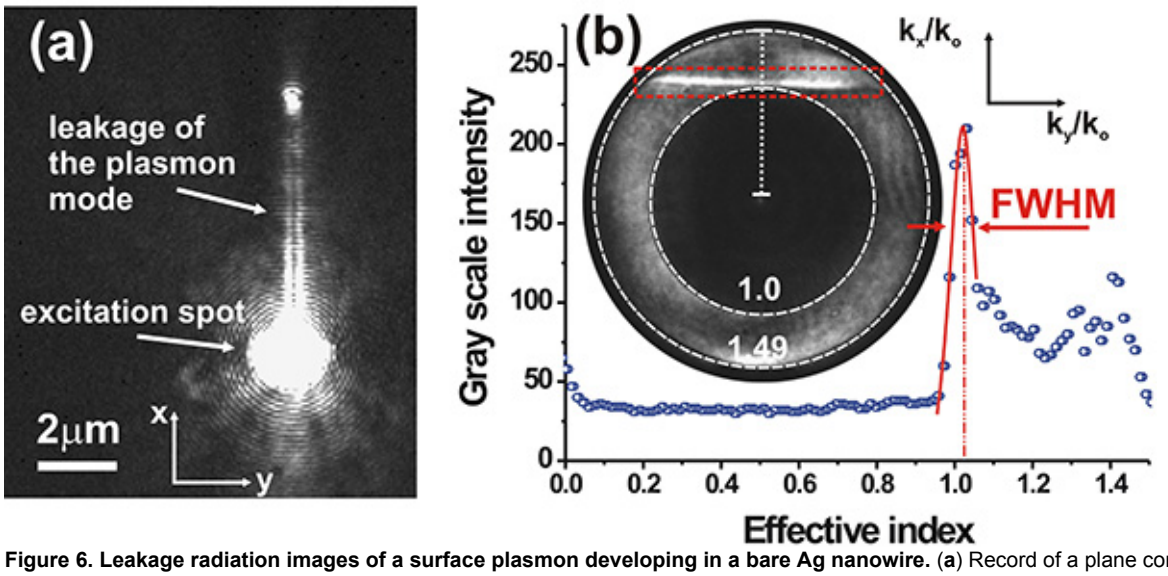

Figure 6. Leakage radiation images of a surface plasmon developing in a bare Ag nanowire. (**a**) Record of a plane conjugate to the object plane. The propagation of the mode is readily seen by detecting its leakage along the nanowire. The excitation spot is the intensity saturated region. (**b**) Intensity distribution recorded in the Fourier plane. This image represents the wave-vector content of the collected light signal. The bright line at a constant k_x/k_o in the red dashed box is the wave-vector distribution of the surface plasmon mode leaking in the substrate. The profile along the k_x/k_o axis (doted line in the Fourier plane) is shown with blue dot. The position of the effective index of the plasmon mode and its propagation length are extracted from a Lorentzian fit through the data (red curve). Here N_{eff}=1.02 and the propagation length is inversely proportional to the full-width at half-maximum (FWHM) of the fit. Click here to view larger image.

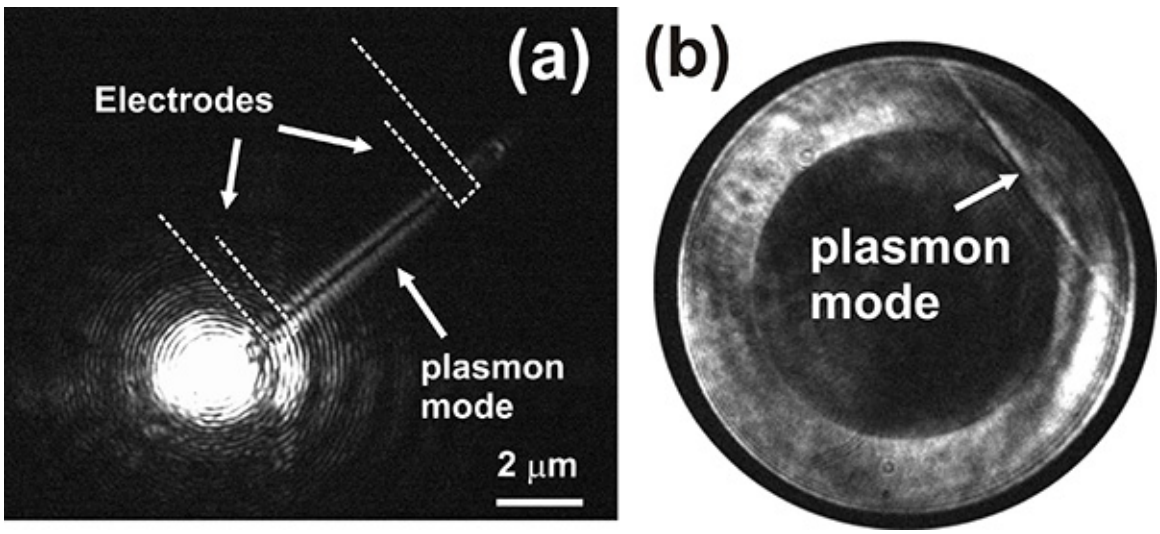

Figure 7. Leakage radiation image of a surface plasmon developing in a Ag nanowire contacted by two electrodes. (**a**) Record of the conjugate object plane. The dashed white lines outline the position of the electrodes. (**b**) Record of the corresponding conjugate Fourier plane. Click here to view larger image.

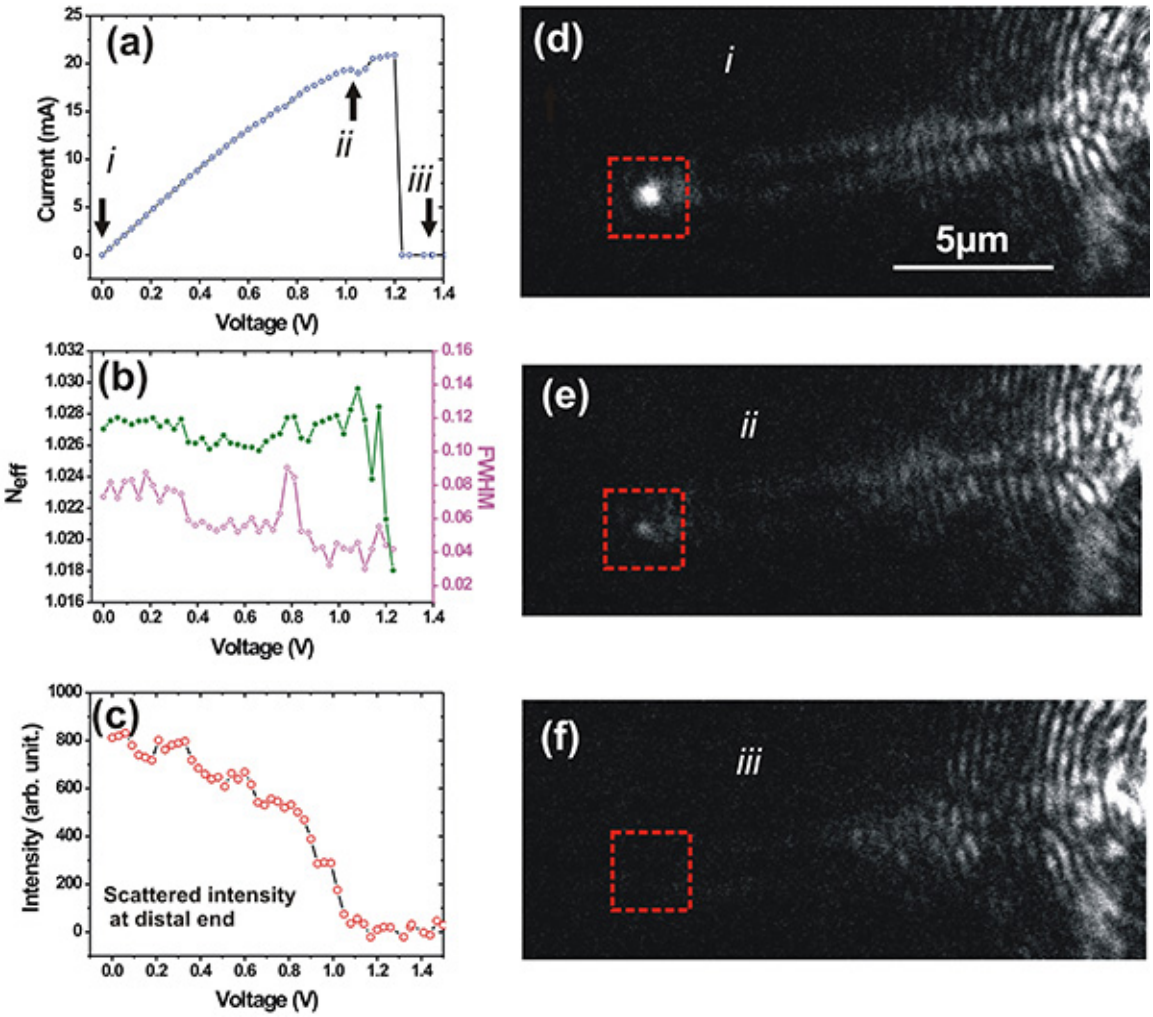

Figure 8. Effect of electron flow on the surface plasmon properties. (**a**) Current-voltage characteristic of a Ag nanowire showing its electromigration-induced breakdown. (**b**) Evolution of the plasmon effective index N_{eff} and the full-width at half-maximum (FWHM) as a function of applied bias. (**c**) Bias-dependence of the intensity signal scattered at the distal end of the nanowire. (**d**) to (**f**) Leakage radiation images taken at different points of the output characteristic labeled *i, ii,* and *iii*, respectively. The intensity level reported in (**c**) is extracted from the red boxes displayed in (**d**) to (**f**). Click here to view larger image.

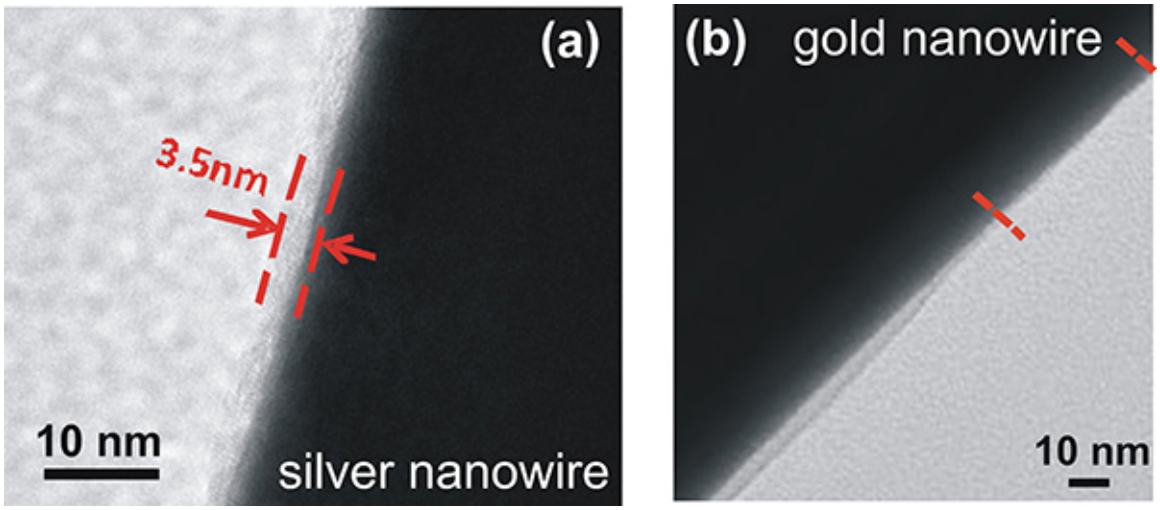

Figure 9. H**igh-resolution transmission electron micrographs showing the presence of surfactant on the surface of the synthesized Ag and Au nanowires.** For silver synthesis (**a**), a 3.5 nm thick surfactant covers the entire surface of the nanowire (arrows). An inhomogeneous coverage of the surface is however typical from Au synthesis (**b**). For instance, the surface of the nanowire located between the two dashed lines is free of surfactant. The presence of the surfactant on the nanowire surface affects the electronic transport. Click here to view larger image.

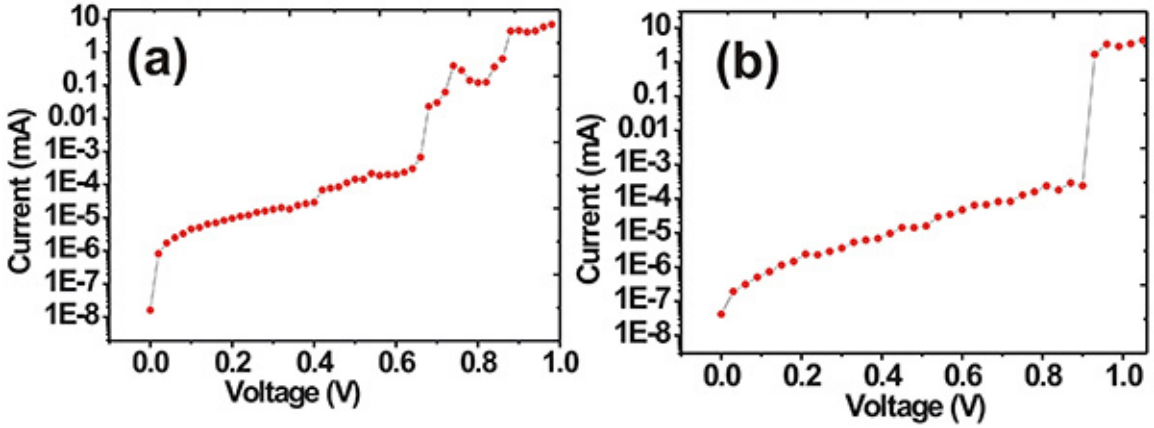

Figure 10. (a) and (b) Current-voltage characteristics for two different connected nanowires during an initial bias sweep (semi-logarithmic scales). In both graphs, sudden current jumps punctuate the curves indicative of a partial destruction of the surfactant layer located between the Au electrodes and the nanowire surface. After burning off the surfactant layer, a subsequent bias sweep typically shows a monotonous characteristic similar to that of **Figure 8(a)**. Click here to view larger image.

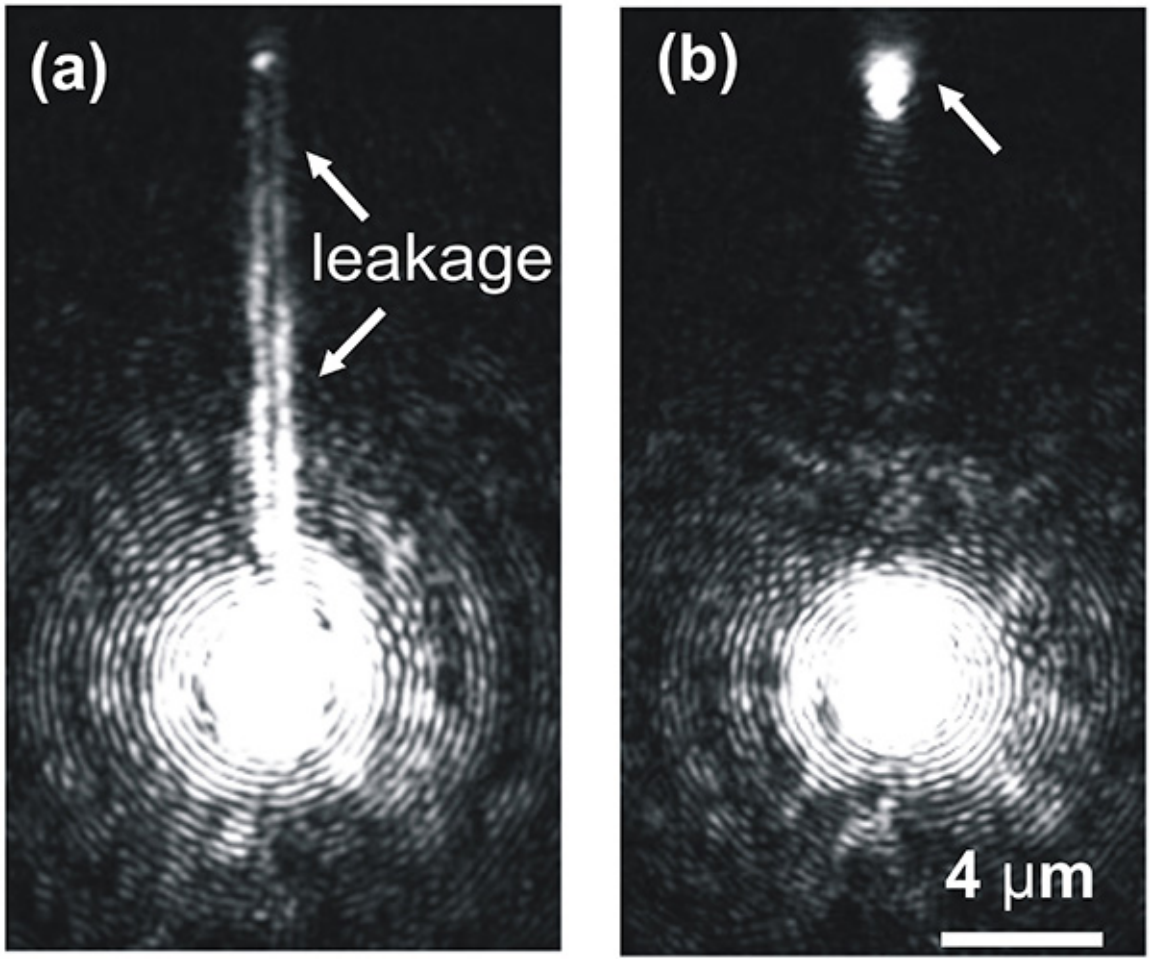

Figure 11. Position-dependent surface plasmon mode excitation. In (**a**), the two luminous light distributed on either side of the nanowire confirms the excitation of leaky surface plasmon mode. In (**b**), the nanowire extremity is slightly displaced in the focal spot to excite the bound surface plasmon. This mode has an effective index greater than the collection angle of the objective and remains undetected during its propagation. However, the presence of a strong signal at the distal end indicates that the bound mode is efficiently scattered out. Click here to view larger image.

Discussion

The synthesis uses an excess of chemical surfactant remaining bound to the surface of the nanowire as illustrated in the transmission electron micrograph of **Figure 9(a)**. This layer creates a dielectric barrier preventing the current to flow through the electrode-nanowire interface. **Figures 10(a)** and **(b)** show typical examples of the current-voltage characteristics. Sharp current steps at certain biases punctuate the curves. These steps occur when the current density in the nanowire is large enough to physically destroy the surfactant layer. An ohmic contact between the electrodes and the nanowire is often established after one to three steps. Typical current values at that conduction point are in the range of 5-10 mA for a bias slightly below 1 V. Special attention should be taken when increasing the bias further. The current densities under this electrical condition can reach the electromigration threshold leading to an irremediable destruction of the nanowire. When an ohmic contact is established, the current/voltage characteristic shows a linear trend indicative of a metal contact (**Figure 8(a)**).

Another point of concern arises when an electrical contact to nanowires thicker that 100 nm is necessary. The protocol to fabricate the electrodes requires working with <70 nm thin Cr/Au layer. This restriction guarantees an optimized ratio between the height of the electron-sensitive resist and the thickness of the evaporated Au layer. A [3:1] ratio is necessary for successfully completing the chemical liftoff. This limited electrode thickness becomes problematic when nanowires with larger radii need to be connected. To overcome this issue, the sampled are mounted on a 50° angled substrate holder in the thermal evaporator. While this approach increases the complexity of the electrode layout (the electrode connecting the nanowire extremities must be oriented along the same direction regardless of nanowire orientations), nanowires with diameter approaching 600 nm are successfully contacted with 70 nm thick electrodes. Because of the angled evaporation, the nanowire shadows the metal flux during the evaporation process and its backside remains unconnected (**Figure 4(b)**).

A similar protocol is deployed for contacting Au nanowires. Au nanowires are fabricated using nitrate ion assisted conventional synthesis[19]. The synthesis forms thinner nanowires with section width ranging from 70-150 nm. For Au nanowires, the current-to-voltage characteristic varies evolves monotonously during the first bias sweep. Transmission electron microscopy conducted on the synthesized Au nanowires reveals an inhomogeneous distribution of the surfactant over the nanowire surface with large portions remaining uncovered as shown in **Figure 9(b)**. The surface of the nanowire located between the two red dashed lines is not covered by the surfactant. The drawback at using gold nanowires is

that the surface plasmon propagation is significantly shorter than in Ag nanowires. Combined with a reduced coupling efficiency resulting from a smaller diameter, shorter nanowires and hence smaller electrode separations are typically required. Leakage images obtained for Au nanowires are therefore difficult to analyze.

An efficient excitation of the nanowire surface plasmon mode critically depends on a series of parameters including the properties of the incident beam and the nanowire geometry. For a diffraction-limited focused beam, the plasmon mode can be excited provided that scattering of the incident field by the nanowire extremity generates a matching wave-vector with the correct polarization symmetry. However, the field distribution inside a tightly focused laser beam is very inhomogeneous and the different in-plane and out of plane field components are spatially separated[20]. This implies that for a given linear polarization state, the excitation efficiency and the nature of the excited surface plasmon mode (leaky or bound) depend on the orientation of the nanowire with respect to the incident polarization and the precise location of its extremity in the focal region. **Figure 11** shows the intensity distribution on the conjugate image plane of the microscope for two slightly different positions of the nanowire extremity inside the focused laser beam. In **Figure 11(a)**, the leaky surface plasmon is excited as shown by the arrow. In **Figure 11(b)**, scattering at the distal end (arrow) indicates the excitation of a bound mode at an effective index greater than the collection angle of the objective. Fine adjustment of the position of the nanowire with the piezoelectric stage is therefore required to optimize the coupling efficiency to the desired surface plasmon mode.

The protocol for electrically contacting metal nanowire described here is very robust against the inevitable stochastic deposition of chemically synthesized colloidal nano to micro-structures. Using the different alignment steps, the position of the electrodes can be determined with an accuracy of approximately 50 nm. A third alignment procedure and a reduced write field during electron-beam lithography would probably provide a higher precision. The protocol however suffers from the large number of steps necessary to realize a basic plasmonic unit and the equipment required to fabricate and characterize the circuitry. Alternatively, direct dip-pen lithography can also be utilized to realize the electrodes mitigating the need for prepatterning and the subsequent alignment steps[21]. Prealignment of the nanowires in well-defined positions would greatly reduce the fabrication time. Currently each sample requires locating the nanowires and designing the corresponding contacting leads. For that purpose, dielectrophoretic trapping[22] could be an asset to reduce the complexity of the electrode layout. While large-scale alignment of nanowires[23] have been demonstrated, the technique requires operating in a liquid environment that may jeopardize the very functionality of a plasmonic circuitry. Furthermore, dielectrophoresis does not mitigate the need for electron-beam lithography to fabricate the leads. Hecht and coworkers recently developed another approach where electrodes and nanowires are fabricated directly by milling a single-crystal Au flake with a focused ion beam[24]. Because of the crystalline nature of the structures the electrical connection to the nanowire is therefore optimum (no defects). This would remove the difficulty to contact the nanowire through the surfactant as discussed in **Figures 9** and **10** and would also increase the maximum current density passing through the nanowire before its electrical breakdown. The technique is however difficult to implement for a large number of nanowires and should be adapted to silver flakes to circumvent the larger plasmon damping of Au nanowires.

Disclosures

The authors declare that they have no competing financial interests.

Acknowledgements

The research leading to these results has received funding from the European Research Council under the European Community's Seventh Framework Program FP7/2007–2013 Grant Agreement no 306772 and Grant ERC-2007-StG No. 203872-COMOSYEL. This work is also partially funded by the Agence Nationale de la Recherche (ANR) under Grant Plastips (ANR-09-BLAN-0049). A. S. thanks a postdoctoral scholarship from the Région de Bourgogne under the PARI program. M.S. acknowledges a stipend from the Chinese Scholarship Council. D.Z. acknowledges support from the National Natural Science Foundation of China for Grants 11004182 and 61036005.

References

1. Ozbay, E. Plasmonics: Merging photonics and electronics at nanoscale dimensions. *Sci.*. **311** (5758), 189 - 193, DOI: 10.1126/science.1114849, (2006).
2. Zia, R., Schuller, J. A., Chandran, A. & Brongersma, M. L. Plasmonics: the next chip-scale technology, *Mater. Today* **9** (7), 20 - 27, DOI: 10.1016/S1369-7021(06)71572-3, (2006).
3. Ebbesen, Th. W. Genet, C. & Bozhevolnyi, S. I. Surface-plasmon circuitry. *Phys. Today*. **61** (5), 44 - 50, DOI:10.1063/1.2930735, (2008).
4. Pyayt, A. L., Wiley, B., Xia, Y., Chen, A. & Dalton, L. Integration of photonic and silver nanowire plasmonic waveguides, *Nat. Nanotechnol.* **3,** 660-665, DOI:10.1063/1.2930735, (2008).
5. Dickson, R. M. & Lyon, L. A. Unidirectional Plasmon Propagation in Metallic Nanowires. *J. Phys. Chem. B*. **104**, 6095-6098, DOI:10.1021/jp001435b, (2000).
6. Kan, C.X., Zhu, J.-J., and Zhu, X.-G. Silver nanostructures with well-controlled shapes-synthesis, characterization and growth mechanism. *J. Phys. D: Appl. Phys.*. **41** (15), 155304, DOI:10.1088/0022-3727/41/15/155304, (2008).
7. Song, M. *et al.* Electron-induced limitation of surface plasmon propagation in silver nanowires. *Nanotechnol.*. **24** (9), 095201, DOI:10.1088/09574484/24/9/095201, (2013).
8. Drezet, A. *et al.* Leakage radiation microscopy of surface plasmonpolaritons. *Mater. Sci. Eng. B*. **148**, 220-229 DOI:10.1016/j.mseb.2007.10.010, (2007).
9. Song, M. *et al*. Imaging Symmetry-Selected Corner Plasmon Modes in Penta-Twinned Crystalline Ag Nanowires. *ACS Nano*. **5** (7), 5874-5880 DOI: 10.1021/nn201648d, (2011).
10. Miljković, V., Shegai, T., Johansson, P. & Käll, M. Simulating light scattering from supported plasmonic nanowires. *Opt. Express*. **20** (10), 10816-10826, DOI:10.1364/OE.20.010816, (2012).

11. Massenot, S. *et al.* Polymer-metal waveguides characterization by Fourier plane leakage radiation microscopy. *Appl. Phys. Lett.*. **91**, 243102, DOI:10.1063/1.2824840, (2007).
12. Ditlbacher, H., *et al.* Silver Nanowires as Surface Plasmon Resonators. *Phys. Rev. Lett.*. **95** (25), 257403, DOI:10.1103/ PhysRevLett.95.257403, (2005).
13. Margueritat, J. *et al.* Influence of the number of nanoparticles on the enhancement properties of surface-enhanced Raman scattering active area: sensitivity versus repeatability. *ACS Nano*. **5**(3), 1630-1638, DOI:10.1021/ nn103256t, (2011).
14. Rivera, T. P., Lecarme, O., Hartmann, J., Rossitto, E., Berton, K. & Peyrade, D. Assisted convective-capillary force assembly of gold colloids in a microfluidic cell: Plasmonic properties of deterministic nanostructures. *J. Vac. Sci. Technol. B*. **26**, 2513-2519, DOI:10.1116/1.3021396, (2008).
15. Cronin, S. B, *et al*. Thermoelectric investigation of bismuth nanowires. *18th international conference on Thermoelectrics*. 554-557, DOI: 10.1109/ICT.1999.843450, (1999).
16. Cronin, S. B., *et al*. Making electrical contacts yo nanowires with a thick oxide coating. *Nanotechnol.*. **13** (5), 653, DOI: 10.1088/0957-4484/16/5/322, (2002).
17. Colas des Francs, G. *et al.* Integrated plasmonic waveguides: A mode solver based on density of states formulation. *Phys. Rev. B*. **80** (11), 115419, DOI: 10.1103/PhysRevB.80.115419, (2009).
18. Stahlmecke, B., *et al.* Electromigration in self-organized single-crystalline silver nanowires. *Appl. Phys. Lett.*. **88** (5), 053122, DOI:10.1063/1.2172012, (2006).
19. Kim, F., Sohn, K., Wu, J. & Huang, J. Chemical Synthesis of Gold Nanowires in Acidic Solutions. *J. American Chem. Soc.*. **130** (5), 14442-14443, DOI: 10.1021/ja806759v, (2008).
20. Novotny, L. & Hecht, B. *Princ. Nano-Opt.*. Cambridge University Press, (2006).
21. Wang, W. M., *et al.* Dip-pen nanolithography of electrical contacts to single-walled carbon nanotubes. *ACS Nano*. **3** (11) 35443-3551, DOI/ 10.1021/nn900984w (2009).
22. Kuzyk, A. Dielectrophoresis at the nanoscale. *Electrophoresis*. **32** (17), 2307-2313, DOI: 10.1002/elps.201100038, (2011).
23. Freer, E. M., Grachev, O., Duan, X., Martin, S., & Stumbo, D. P. High-yield self-limiting single-nanowire assembly with dielectrophoresis. *Nat. Technol.*. **5**, 525-530, DOI: 10,1038/nnano.2010.106 (2010).
24. Huang, J-S., *et al.* Atomically-flat single-crystalline gold nanostructures for plasmonic nanocircuitry. *Nat. Comm.*. **1**, 150, DOI:10.1038/ ncomms1143 (2010).

